A new calibration code for the JET polarimeter

M. Gelfusa,[1] A. Murari,[2] P. Gaudio,[1] A. Boboc,[3] M. Brombin,[2] F. P. Orsitto,[4] E. Giovannozzi,[4] and JET EFDA Contributors[5,a)]
[1]*Associazione EURATOM-ENEA–University of Rome "Tor Vergata," 00133 Roma, Italy*
[2]*Consorzio RFX Associazione EURATOM-ENEA per la Fusione, 4-35127 Padova, Italy*
[3]*EURATOM/CCFE Fusion Association, Culham Science Centre, Abingdon OX14 3DB, United Kingdom*
[4]*Associazione EURATOM-ENEA–CR Frascati, Frascati 00044, Italy*
[5]*JET-EFDA, Culham Science Centre, Abingdon OX14 3DB, United Kingdom*

(Received 8 December 2009; accepted 19 April 2010; published online 28 May 2010)

An equivalent model of JET polarimeter is presented, which overcomes the drawbacks of previous versions of the fitting procedures used to provide calibrated results. First of all the signal processing electronics has been simulated, to confirm that it is still working within the original specifications. Then the effective optical path of both the vertical and lateral chords has been implemented to produce the calibration curves. The principle approach to the model has allowed obtaining a unique procedure which can be applied to any manual calibration and remains constant until the following one. The optical model of the chords is then applied to derive the plasma measurements. The results are in good agreement with the estimates of the most advanced full wave propagation code available and have been benchmarked with other diagnostics. The devised procedure has proved to work properly also for the most recent campaigns and high current experiments. [doi:10.1063/1.3427504]

I. INTRODUCTION

Thermonuclear plasmas are active and anisotropic media, which strongly affect the propagation of electromagnetic radiation, depending on their parameters. The measurement of the change in the polarization state (Faraday rotation and Cotton–Mouton effect) of a laser beam probing a plasma can therefore provide very useful information about various physical quantities crucial for both the understanding of the physics and the control of the configuration. As a consequence, polarimetric diagnostics have become quite common in experiments studying nuclear fusion plasmas. Typically in polarimetry a linearly polarized laser beam probes the plasma and its polarization output is compared with the initial one.

On JET, a dual interferometer/polarimeter system carries out, routinely, the Faraday rotation and Cotton–Mouton effect measurements. On JET these measurements are complicated by two facts: first the general issue of the nonlinear interaction between the Faraday rotation and the Cotton–Mouton effect and second a "spurious" phase shift induced by nonidentified optical components of the diagnostic. The effect of this spurious instrumental phase shift must be taken into account in the calibration and signal processing procedures.

Since the optical components introducing the spurious effects are completely unknown, then the previous calibration procedure has been based on an empirical model in which purely numerical and quite complex fitting procedures are implemented to evaluate the calibration parameters and the polarimetric measurements. This processing method has been developed without any investigation on the source of the spurious effect and it works as a black box without a clear relation with the hardware setup. A statistical analysis, carried out on the polarimetric measurements acquired during the campaigns 2003–2009, has highlighted some calibration problems affecting mainly the experimental data of the most recent campaigns (2008–2009) particularly those of the high current discharges. Therefore, it has been decided to develop a new calibration code, based on the layout and therefore on the optical setup of the diagnostic.

This new calibration code is based on the description of the laser beam propagation through a series of optical components, modeled with the well-known Mueller matrix formalism.[1] The quality of the new calibration code has been tested by comparing the experimental values of the Faraday rotation and the Cotton–Mouton phase shift, obtained with the new calibration procedure, with the numerical estimates of the same quantities provided by a full wave propagation code, explicitly developed to validate the calibration method.

The paper is organized as follows: In Sec. II, after a brief description of JET interferometer/polarimeter system, a simulator developed to verify the correct operation of the signal processing electronics is presented; in Sec. III the new calibration code for the vertical and the lateral chords is described; in Sec. IV a general description of the full wave propagation code is provided and in Sec. V the obtained results are reported.

II. JET INTERFEROMETER/POLARIMETER

A. Polarimetric measurements

Two separate phenomena influence the polarization of the Far infrared (FIR) beam that passes through a magnetically confined plasma:[2]

[a)]See the Appendix of F. Romanelli *et al.*, Proceedings of the 22nd IAEA Fusion Energy Conference, Geneva, Switzerland, 2008 and the Appendix of Nucl. Fusion **49**, 104006 (2009).

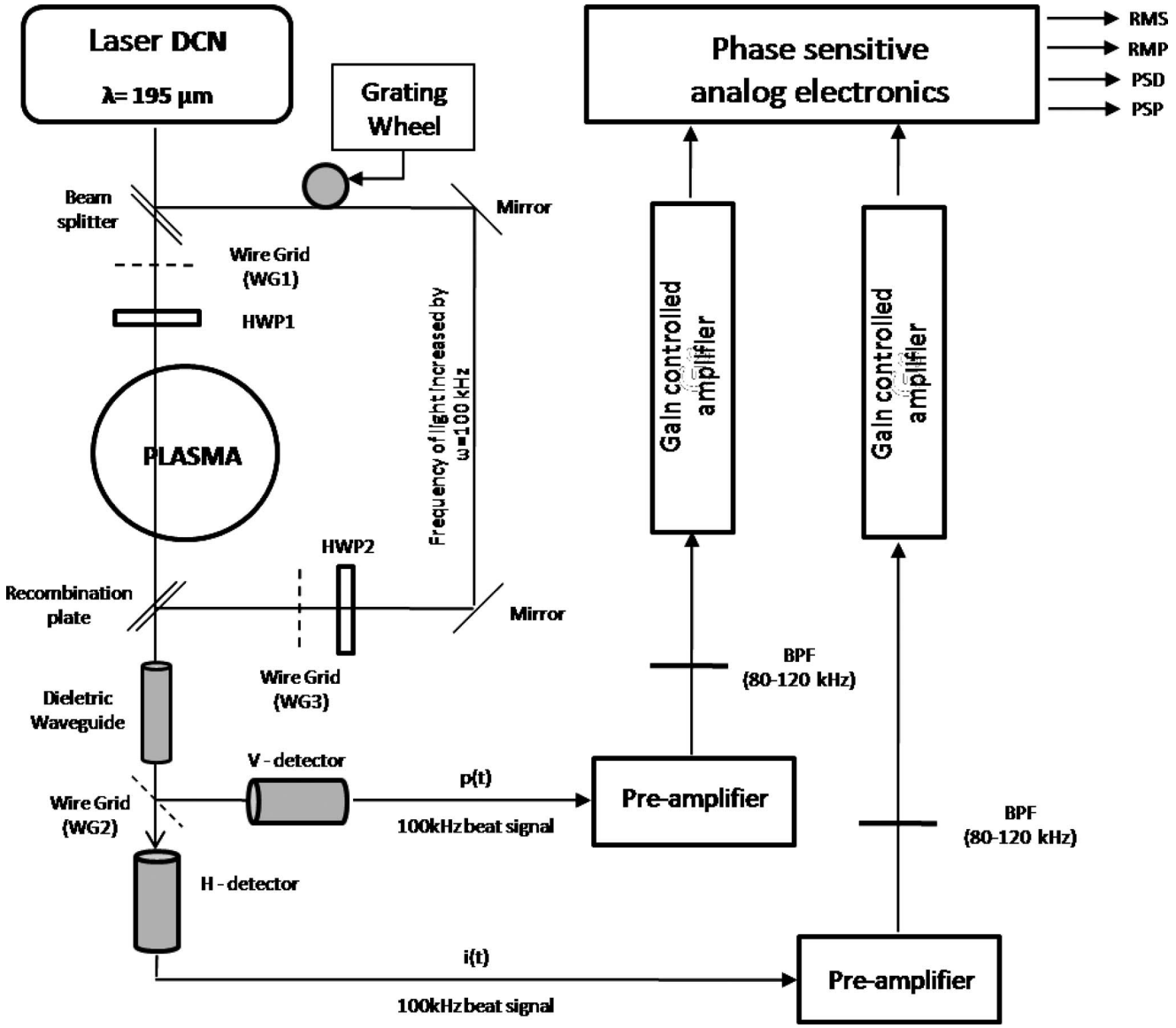

FIG. 1. Schematic of the polarimeter vertical chords.

- Faraday rotation effect: The plane of linearly polarized light passing through a plasma is rotated when a magnetic field is applied parallel to the direction of propagation according to the relation

$$\Delta\Psi \propto \lambda^2 \int n_e \cdot B_{\amalg} \cdot dz. \quad (1)$$

- Cotton–Mouton effect: The ellipticity acquired by a linearly polarized light passing through a plasma is dependent on the density and the magnetic field perpendicular to the direction of propagation.

$$\Phi \propto \lambda^3 \int n_e \cdot B_{\perp}^2 \cdot dz. \quad (2)$$

Here λ is the laser wavelength, n_e is the plasma electron density, and $B_{\amalg}$ and $B_{\perp}$ the parallel and perpendicular components of the magnetic field, respectively. After traversing the plasma a polarized beam suffers a rotation of the polarization plane due to Faraday rotation and acquires ellipticity due to the Cotton–Mouton effect.

B. Description of the diagnostic

At JET, the FIR diagnostic operates as a dual interferometer/polarimeter system.

The system consists of four vertical and four lateral laser beams, which provide measurements of the line-integrated plasma density by means of interferometry and Faraday rotation angle and Cotton–Mouton effect by polarimetry.[3,4] The radiation, provided by a Deuterium Cyanide laser at 195 μm, is split into a probing beam and a reference beam, which is modulated by a rotating wheel at 100 kHz.

After the vessel, the probing and the reference beam are recombined (with a recombination quartz plate) and then they reach a wire grid which divides the electric field into two orthogonal directions that are focused onto two InSb He-cooled detectors. The schematic layout of the system, for one vertical chord, is shown in Fig. 1.

The Faraday rotation angle is measured on all eight channels by evaluating the two components of polarization of the laser beam that passes through the plasma. These mea-

surements are preceded by an online calibration performed before each shot (using half-wave plates).[3,4] In order to measure the Cotton–Mouton angle, a special setup, with initial linear polarization of the input beam set at 45° with respect to the toroidal field direction (x-axis) for the vertical channels and parallel to the toroidal field for the horizontal channels, has been implemented.

The grid and half-wave plate before the entrance window are used to set the required direction of the linear input polarization. In the calibration phase this half-wave plate is rotated before each discharge to simulate the Faraday rotation effect.

The amplitudes of the measured beat signals are proportional to the orthogonal components of the corresponding electric field vector amplitudes of the electromagnetic wave in the local coordinate system[4] defined by the orientation of the wire grid in front of the detectors

$$p(t) \propto E_y \cos(\omega_0 t - \varphi) = E_y^0 \sin \Theta \cdot \cos(\omega_0 t - \varphi), \tag{3}$$

$$i(t) \propto E_x \cos(\omega_0 t) = E_x^0 \cos \Theta \cdot \cos(\omega_0 t), \tag{4}$$

where ω_0 is the modulation frequency (100 kHz) obtained by a rotating grating wheel, φ is the phase shift between the orthogonal components, E_x and E_y are the components of the electrical vector, and $\Theta = \Theta_0 + \alpha$ with $\Theta_0 = 45°$. In presence of plasma α represents the Faraday angle; during the calibration it is equal to twice the rotation angle of the half-wave plate.

The amplified signals are sent to a phase sensitive electronic module to produce four additional signals that are sent to the data acquisition system.

C. Signal processing electronics

The present electronics used to process data from the detectors of the JET FIR polarimeter has been commissioned in 2002. Since in the past years the diagnostic has been configured for measuring routinely both the Faraday rotation effect and the Cotton–Mouton effect with a different optical setup, it becomes important to check the performance of the analog phase sensitive electronics.[5–7]

The main operations performed by the analog electronics of the polarimeter have been implemented via software using both SIMULINK and MATLAB. This allows an accurate characterization of the instrument and an assessment of the quality of the provided measurements. The detected signals [$i(t)$ and $p(t)$] are processed by analog phase sensitive electronics to obtain the following measurements: RMS, RMP, PSP, and PSD:

$$RMS = \langle i(t) \times i(t) \rangle, \tag{5}$$

$$RMP = \langle i'(t) \times i'(t) \rangle, \tag{6}$$

$$PSD = \langle i(t) \times p(t) \rangle, \tag{7}$$

$$PSP = \langle i'(t) \times p(t) \rangle, \tag{8}$$

where $i'(t) \propto \sin(\omega_0 t)$ is generated by shifting of 90° the phase of the $i(t)$ signal.

These four signals are processed by a code to obtain the two ratios R and R' which are related to polarimetric parameters of the radiation after the plasma

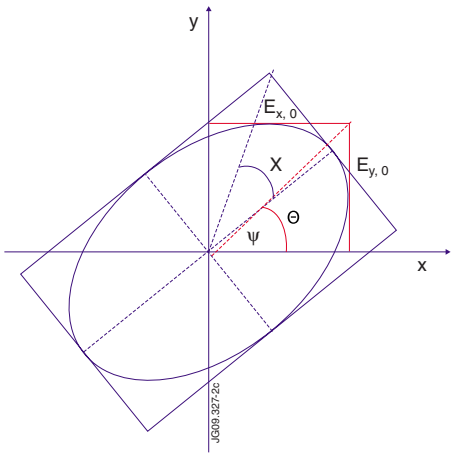

FIG. 2. (Color online) The polarization ellipse is often adopted to represent the relation between the electrical and the geometrical parameters of the polarized radiation.

$$R = \frac{PSD}{RMS} = C^{-1} \tan(\Theta) \cdot \cos \varphi, \tag{9}$$

$$R' = \frac{PSP}{\sqrt{RMS \cdot RMP}} = C^{-1} \tan(\Theta) \cdot \sin \varphi, \tag{10}$$

where C is a calibration factor.

Given the two ratio R and R', the main parameters of the electrical vector of the polarized radiation can be derived

- the phase shift

$$\varphi = \text{arctag} \frac{R'}{R} = \phi_0 + \Phi, \tag{11}$$

  where ϕ_0 is the phase shift between the two signals in absence of plasma, while Φ represents the angle introduced by the Cotton–Mouton effect.
- the ratio Θ between the orthogonal components of the electrical vector

$$R^2 + R'^2 = C^{-2} \tan^2 \Theta \Rightarrow \tan^2 \Theta = C^2(R^2 + R'^2). \tag{12}$$

The optical properties of the polarized light, polarization angle (ψ), and ellipticity ($\varepsilon = \tan \chi$) can be derived using the well known identities which relate the electrical parameters to the geometrical ones

$$\tan(2\psi) = \tan(2\Theta)\cos \varphi, \tag{13}$$

$$\sin(2\chi) = \sin(2\Theta)\sin \varphi. \tag{14}$$

The parameter ψ is the polarization angle between the major axis of the polarization ellipse (see Fig. 2) and the reference x-axis; the parameter χ is related to the ellipticity of the radiation.

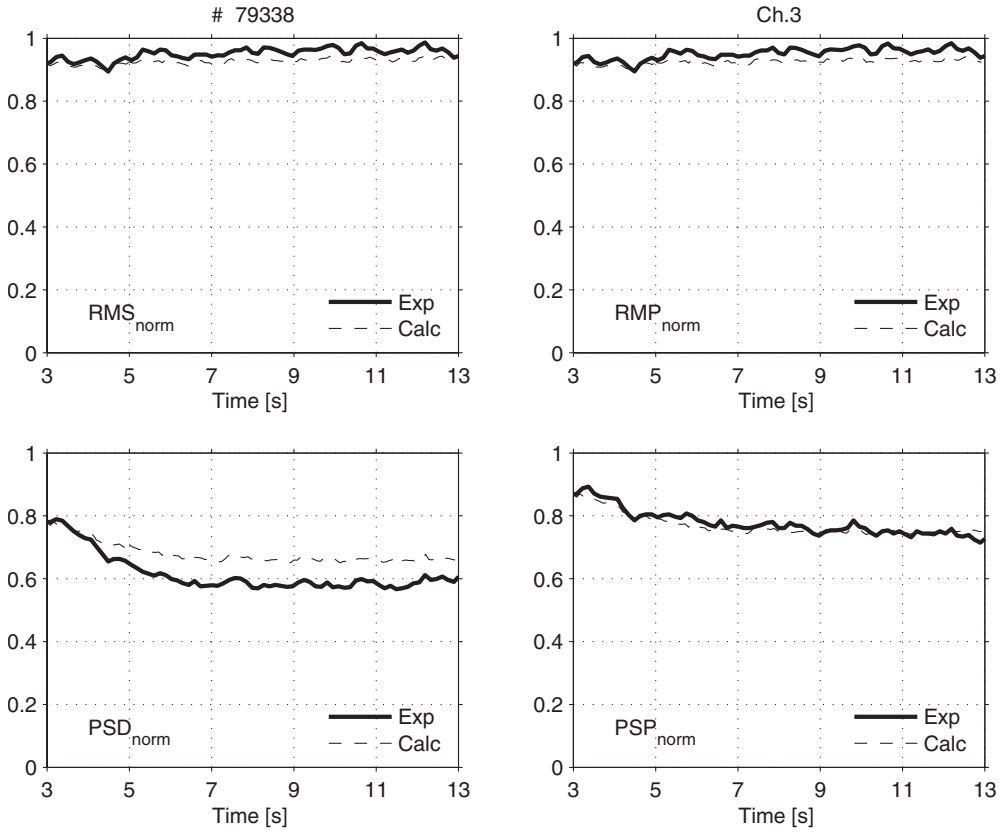

FIG. 3. Comparison between the normalized experimental signals RMS, RMP, PSP, PSD (continuous line), and the estimates of the MATLAB electronics simulator (dashed line).

1. Electronics bench test: hardware setup and data processing

The tests to check the reliability of the electronic cards used on polarimetry have mainly consisted on acquiring the raw data after the detectors, process them via software, and then compare the obtained outputs with the ones given by the polarimeter electronics. The first test has been performed getting the raw signals after the bandpass filter (80–120 kHz) before the phase analog sensitive detector (see Fig. 1). Then the data have been processed by an electronic simulator implemented with SIMULINK. For the second and more recent test the data have been taken after the detectors, before the bandpass filter. This second set of signals has been analyzed with a MATLAB code, which implements the bandpass filter and the main operations of the phase sensitive detector [Eq. (5)–(8)].

From Fig. 3 it is clear the good agreement between the simulated signals and the real ones provided by the electronics of the polarimeter. This confirms that the phase sensitive detector is still working properly within its design parameters.

III. CALIBRATION PROCEDURE

At JET an online calibration, to link the output voltage of the detectors to the effective Faraday rotation angle, is carried out, for each chord, before each shot.

Currently, the procedure of calibration is the following: the half-wave plate, located at the entrance of the vacuum vessel (see Fig. 1), is rotated (via a step motor) of a well-known angle (α) and the phase shift (φ) is recorded at each angle, while the Faraday rotation (2α) is equal to twice the half-wave plate angle.

Moreover, before each campaign, or when it is necessary, a manual calibration is performed. It consists of the rotation of the wire grid, located in front of the two detectors, to optimize the signals detected.

Figures 4 and 5 show examples of the calibration curves for the vertical chord no. 3. Figure 4 represents the Faraday angle as function of the time. Figure 5 shows the phase shift versus the half-wave plate rotation.

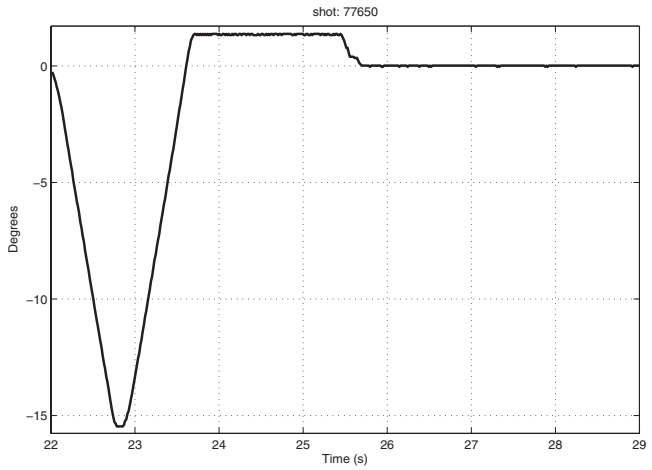

FIG. 4. Calibration curve of the Faraday rotation (shot: 77650 chord no. 3). The error bar on the Faraday rotation is of the order of 0.2°.

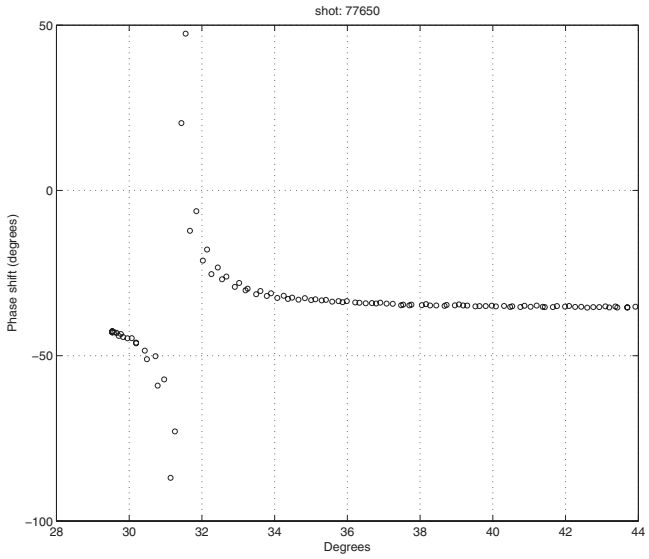

FIG. 5. Phase shift calibration curve (shot: 77650 chord no. 3). The error bar on the phase shift is of the order of 2°.

From Fig. 5 it is clear that the value of the phase shift is not constant when the half-wave angle is varied, as it would be expected for a system with only ideal optical components. Because of this nonideal behavior, at JET the polarimetric signals are processed using a model which assumes that an unspecified optical element generates a "*spurious ellipticity*" characterized by a constant phase shift referred to a rotated coordinate system of unknown orientation.[4]

A. New calibration code for the vertical chords

As mentioned, a new calibration code has been developed to provide a more robust calibration procedure valid over the whole range of JET discharges. In the new code, the path of the laser beam is described by a series of optical components modeled using the Mueller matrix formalism.

Referring to the polarimeter schematic reported in Fig. 1, the optical components involved in the model are: the half-wave plate, the wire grid located in front of the detectors, and a cascade of two retarders to reproduce the spurious ellipticity which afflicts the polarimetry measurements. A systematic analysis was performed showing very clearly that the additional optical components presently modeled are sufficient to account for the spurious ellipticity. Adding additional components did not improve the fit of the calibration curves. The location of the two retarders after the plasma is motivated by the fact that only optical components between the output grid and the detectors have a sufficiently strong influence.

The calibration of Faraday angle is carried out rotating the half-wave plate, in absence of plasma, by a known angle (α). So, the Mueller matrix for this component is[8,9]

$$M_\alpha = \begin{vmatrix} 1 & 0 & 0 & 0 \\ 0 & \cos 2\alpha & \sin 2\alpha & 0 \\ 0 & -\sin 2\alpha & \cos 2\alpha & 0 \\ 0 & 0 & 0 & 1 \end{vmatrix}, \tag{15}$$

which represents the matrix of an ideal rotator. It is primarily used just to change the polarization direction of the beam without modifying the ellipticity.

The two retarders introducing the spurious ellipticity have been modeled with their correspondent Mueller matrices, which in the case of an ideal retarder with a phase shift (δ_1) and its fast axis along x, is

$$M_{\delta_1} = \begin{vmatrix} 1 & 0 & 0 & 0 \\ 0 & 1 & 0 & 0 \\ 0 & 0 & \cos\delta_1 & \sin\delta_1 \\ 0 & 0 & -\sin\delta_1 & \cos\delta_1 \end{vmatrix}. \tag{16}$$

If the fast axis of the retarder is rotated by an angle α_1 from x, the Mueller matrix is

$$M'_{\delta_1} = R(\alpha_1) \cdot M_{\delta_1} \cdot R(-\alpha_1), \tag{17}$$

where $R(\alpha_1)$ is a rotation matrix.

$$R_{\alpha_1} = \begin{vmatrix} 1 & 0 & 0 & 0 \\ 0 & \cos 2\alpha_1 & \sin 2\alpha_1 & 0 \\ 0 & -\sin 2\alpha_1 & \cos 2\alpha_1 & 0 \\ 0 & 0 & 0 & 1 \end{vmatrix}. \tag{18}$$

For the second retarder the Mueller matrix therefore is

$$M'_{\delta_2} = R(\alpha_2) \cdot M_{\delta_2} \cdot R(-\alpha_2). \tag{19}$$

To estimate the phase shift values (δ_1 and δ_2) and the angles at which the retarders are located (α_1 and α_2) in the torus coordinate system, an optimization routine has been written. For each chord, the routine finds the values of these four quantities which allow to best fit the phase shift curve, shown in Fig. 5.

The last optical component involved in the calibration code is the wire grid, which acts as an analyzer, dividing the electric field components into two directions x and y, which are focused onto the corresponding detectors.

Assuming an ideal behavior of the analyzer, the Mueller matrices for transmission and reflection, M_T and M_R, can be written

$$M_T = p_x^2 \cdot \begin{vmatrix} p_x^2+p_y^2 & p_x^2-p_y^2 & 0 & 0 \\ p_x^2-p_y^2 & p_x^2+p_y^2 & 0 & 0 \\ 0 & 0 & 2\cdot p_x\cdot p_y & 0 \\ 0 & 0 & 0 & 2\cdot p_x\cdot p_y \end{vmatrix}, \tag{20}$$

$$M_R = p_y^2 \cdot \begin{vmatrix} p_x^2+p_y^2 & p_x^2-p_y^2 & 0 & 0 \\ p_x^2-p_y^2 & p_x^2+p_y^2 & 0 & 0 \\ 0 & 0 & 2\cdot p_x\cdot p_y & 0 \\ 0 & 0 & 0 & 2\cdot p_x\cdot p_y \end{vmatrix}, \tag{21}$$

where p_x and p_y are, respectively, the cosine and the sine of the wire grid angle.

In ideal conditions, the wire grid should be at 45° with respect to the propagation direction of the radiation, dividing the electric field into the directions x and y.

Looking at the two detector signals, it is possible to estimate the angle between the wires and the incidence electric field of the radiation. As it is shown in Fig. 5, there is an

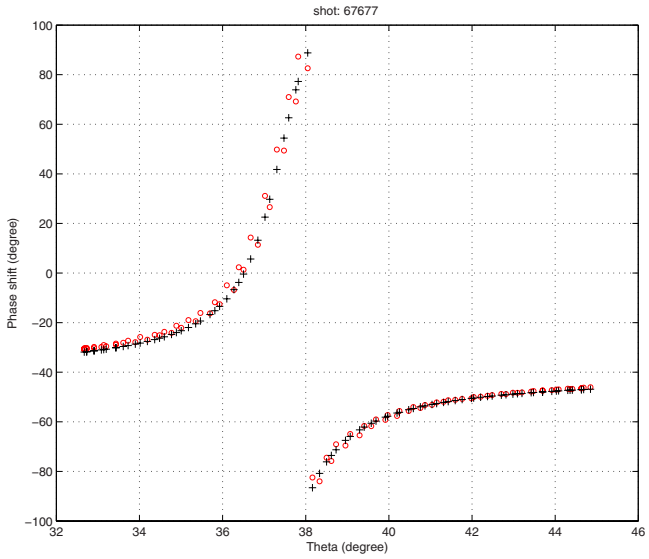

FIG. 6. (Color online) Comparison between the experimental calibration curve (circles) and the estimate of the new calibration model (crosses). Shot: 67677 chord no. 3.

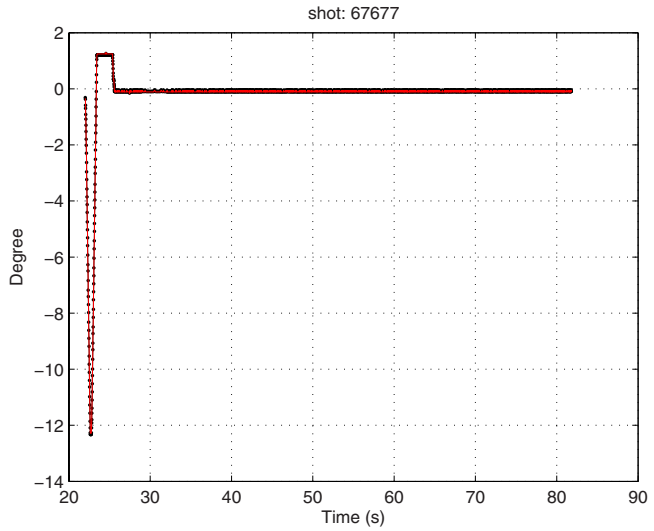

FIG. 7. (Color online) Calibration curve of Faraday angle (shot: 67677 chord no. 3). Comparison between the experimental calibration curve (dotted line) and the estimate of the new calibration model (continuous line).

angle of the polarization for which the phase shift diverges to $\pm\infty$. Since this corresponds to a polarization for which the R signal equals zero and therefore $p(t)$ signal equals zero, it means that all the radiation is collected by the $i(t)$ detector. This condition is verified when the wires are parallel to the direction of $p(t)$ signal. Then the position of the wire with respect to the incidence electric field can be estimated as

$$\alpha_{WG2} = 90 - \alpha_0. \tag{22}$$

After this component, the laser beam is divided in two parts and the corresponding Stokes vectors are given by

$$\vec{S}_{1,R} = M_R \cdot M'_{\delta_2} \cdot M'_{\delta_1} \cdot M_\alpha \cdot \vec{S}_0, \tag{23}$$

$$\vec{S}_{1,T} = M_T \cdot M'_{\delta_2} \cdot M'_{\delta_1} \cdot M_\alpha \cdot \vec{S}_0. \tag{24}$$

The final Stokes vector $(\vec{S}_1)$ is the combination of these two Stokes vectors.

Therefore, it is possible to know the polarization angle and the phase shift, given by

$$\psi = \frac{1}{2}\text{arctag}\left(\frac{S_2}{S_1}\right), \tag{25}$$

$$\Phi = \text{arctag}\left(\frac{S_3}{S_2}\right), \tag{26}$$

where S_1, S_2, and S_3 are the component of the final Stokes vector $(\vec{S}_1)$.

These parameters are linked to the Faraday rotation angle (Ψ) and to the Cotton–Mouton effect (Φ) by

$$\Psi = \psi - \Theta_0, \tag{27}$$

$$\Phi = \varphi - \phi_0. \tag{28}$$

In the following Figs. 6 and 7, the fits of the experimental calibration curves obtained with the new calibration code are reported.

B. New calibration code for the lateral chords

In the following figure the layout of JET polarimeter for a lateral chord is shown.

From Fig. 8, it is clear that is not possible to apply directly the calibration code, developed for the vertical channels, to the horizontal lines of sights because the laser path for the lateral chords is different.

In this case, the radiation passes through the plasma and then it is reflected back using a mirror located on the inner wall. So, in the calibration code this additional optical component has been introduced, which is described by the following Mueller matrix:

$$M_\varepsilon = \begin{vmatrix} 1 & 0 & 0 & 0 \\ 0 & \cos 2\varepsilon & \sin 2\varepsilon & 0 \\ 0 & -\sin 2\varepsilon & \cos 2\varepsilon & 0 \\ 0 & 0 & 0 & 1 \end{vmatrix}, \tag{29}$$

which represents the matrix of an ideal rotator. In the case of the polarimeter lateral chords it has been found that the matrix of an ideal mirror, with ε equal to 180°, is more than adequate to obtain satisfactory results.

The other components involved in the model are the same considered for the vertical chords: the half-wave plate, the wire grid located in front of the detectors, and the two retarders introduced to reproduce the spurious ellipticity.

So, for the horizontal chords, the Stokes vectors after the wire grid (WG2) are given by

$$\vec{S}_{1,R} = M_R \cdot M'_{\delta_2} \cdot M'_{\delta_1} \cdot M_\varepsilon \cdot M_\alpha \cdot \vec{S}_0, \tag{30}$$

$$\vec{S}_{1,T} = M_T \cdot M'_{\delta_2} \cdot M'_{\delta_1} \cdot M_\varepsilon \cdot M_\alpha \cdot \vec{S}_0, \tag{31}$$

where the matrices M_T, M'_{δ_2}, M'_{δ_1}, and M_α are the same as the ones seen in the previous section.

Since the only difference with respect to the vertical chords is the presence of the mirror, which can be easily modeled with a fixed Mueller matrix, the new calibration procedure and the subsequent elaboration of the raw data, to

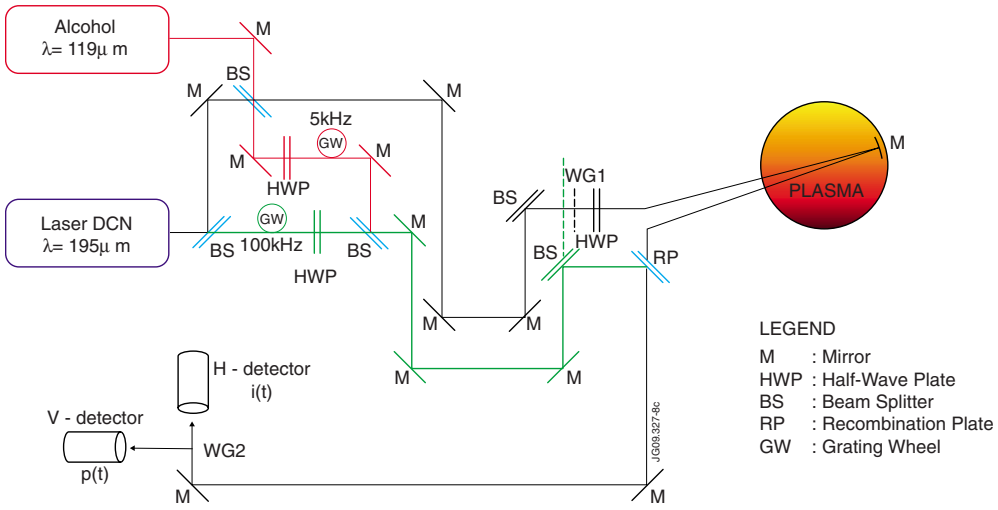

FIG. 8. (Color online) Schematic of the polarimeter horizontal chords.

evaluate the Faraday rotation and the phase shift angle, are the same as for the vertical channels. Again only four quantities (the phase shift values δ_1 and δ_2 and the angles at which the retarders are located α_1 and α_2 in the torus coordinate system) have to be determined with a series of scans.

IV. THE NUMERICAL CODE TO SIMULATE THE EVOLUTION OF THE LASER BEAM POLARIZATION STATE

To confirm the validity of the polarimeter optical model, developed to interpret the calibration data, a numerical code has been implemented, which calculates the evolution of the state of polarization of a laser beam crossing JET plasmas. This code is based on the Stokes formalism and has been particularized for both the horizontal and the vertical chords of JET polarimeter. Starting from the Lidar Thomson scattering density profiles and the equilibrium magnetic field as input, this code gives as output the Faraday rotation angle and the Cotton–Mouton effect. The main equations implemented in the code and the basic validation of the results are reported in this section.

As it is well known,[10,11] the radiation propagating in a magnetized plasma in the absence of dissipation is described by the vector equation[8,12]

$$\frac{d\vec{s}}{dz} = \vec{\Omega} \times \vec{s}, \tag{32}$$

where the Ω vector is expressed as

$$\vec{\Omega} = ka(\Omega_1, \Omega_2, \Omega_3) \tag{33}$$

and the three components are equal to

$$\begin{aligned} \Omega_1 &= C_1 n_e (B_x^2 - B_y^2), \\ \Omega_2 &= 2 \cdot C_1 n_e B_x B_y, \\ \Omega_3 &= C_3 n_e B_z, \end{aligned} \tag{34}$$

where $B_x(z)$, $B_y(z)$, and $B_z(z)$ are the magnetic field components expressed along the laser beam propagation direction (z), n_e is the electronic density (m^{-3}), $C_1 = 1.74 \times 10^{-22}$ and $C_3 = 2 \times 10^{-20}$ are constants (calculated for the laser wavelength of 195 μm of JET polarimeter), and $Z = z/ka$ is the normalized coordinate with respect to the vertical position z of the chord number i, with k the elongation and a the minus radius of the tokamak.[13]

Then, using Eqs. (34), the propagation equation can be written as

$$\begin{aligned} \dot{s}_1 &= \Omega_2 s_3 - \Omega_3 s_2 = 2C_1 n_e B_x B_y s_3 - C_3 n_e B_z s_2, \\ \dot{s}_2 &= -\Omega_1 s_3 + \Omega_3 s_1 = -C_1 n_e (B_x^2 - B_y^2) s_3 + C_3 n_e B_z s_1, \\ \dot{s}_3 &= \Omega_1 s_2 - \Omega_2 s_1 = C_1 n_e (B_x^2 - B_y^2) s_2 - 2C_1 n_e B_x B_y s_1. \end{aligned} \tag{35}$$

The evaluation of the vector $\vec{\Omega} = ka(\Omega_1, \Omega_2, \Omega_3)$ is performed in this work using the electron density profile measured by the Lidar Thomson scattering, while the magnetic field is evaluated using the equilibrium reconstruction of Equilibrium Fitting with only the magnetic measurements.

A. Stokes model solution for the vertical chords

In the case of the vertical chords, the laser beam propagates vertically in a poloidal plane of JET. In this configuration the toroidal magnetic field $(\vec{B}_t)$ is perpendicular to this plane and then it is possible to write Eqs. (34) in the following way:

$$\begin{aligned} \Omega_1 &= C_1 n_e (B_r^2 - B_t^2), \\ \Omega_2 &= 2 \cdot C_1 n_e B_r B_t, \\ \Omega_3 &= C_3 n_e B_v, \end{aligned} \tag{36}$$

where B_r is radial component of the magnetic field, orthogonal to the propagation direction, B_t the toroidal component of the magnetic field, and B_v is the magnetic field along the propagation direction, the vertical axis in the case of this configuration.

Under these conditions Eqs. (35) can be written as[10]

TABLE I. Results of the statistical analysis for the phase shift of the vertical chords. The percentages represent the cases for which the difference between the estimate of the code and the experimental value is equal or less than one fringe (1.14×10^{19} [m^{-2}]).

Less than or equal to one fringe error (%)			
Chord	No. 2	No. 3	No. 4
CM_th-interferom.	68	95	85

$$\dot{s}_1 = \Omega_2 s_3 - \Omega_3 s_2 = 2C_1 n_e B_r B_t s_3 - C_3 n_e B_v s_2,$$

$$\dot{s}_2 = -\Omega_1 s_3 + \Omega_3 s_1 = -C_1 n_e (B_t^2 - B_r^2) s_3 + C_3 n_e B_v s_1, \quad (37)$$

$$\dot{s}_3 = \Omega_1 s_2 - \Omega_2 s_1 = C_1 n_e (B_t^2 - B_r^2) s_2 - 2C_1 n_e B_r B_t s_1.$$

On JET, to maximize the Cotton-Mouton effect on the vertical chords, a linear polarizer has been set at 45° with respect to the toroidal direction. For this geometric configuration of the diagnostic, the initial Stokes vector is defined by

$$s_0 = (0,1,0). \quad (38)$$

Integrating Eqs. (37) with this initial condition, the approximate Stokes equation assumes the following form:[11]

$$s(z) \approx (-W_3, 1, W_1). \quad (39)$$

Usually, in a tokamak the toroidal field is about two orders of magnitude larger than the radial field, so the phase shift can be calculated as

$$\frac{s_3}{s_2} \cong W_1 \cong \int_{z_0}^{z} n(z') B_t^2 dz'. \quad (40)$$

This relation shows the dependence of the Cotton–Mouton effect on the line-integrated electronic density and the toroidal field in a tokamak. This dependence has been used, in this paper, to compare the outputs model with the interferometer measurements to validate the numerical propagation code for the vertical channels.

The propagation code developed has been validated comparing the density estimated from the Cotton–Mouton angle with the interferometry density measurements. Since the lines of sight of the two diagnostics are identical, the line integrated densities should be the same.

The statistical analysis, summarized in the Table I, of all vertical chords permits to deduce that there is a good agreement between the model outputs and the interferometry experimental data.

B. Stokes model solution for the lateral chords

The same analysis has been carried out for all lateral chords. Starting from the propagation equation for the geometry of the lateral chords, a comparison of theoretical outputs and experimental data can be performed. In this case a first validation can be obtained comparing the Faraday angle estimated with the interferometry electron density measurements.

On the lateral chords, the laser beam enters in to the torus chamber of JET facility with an initial linear polarization at 0° with respect to the toroidal field direction.

Thus, in this case, the propagation Eq. (32) assumes the form

$$\dot{s}_1 = 2C_1 n_e B_x B_y s_3 - C_3 n_e B_z s_2,$$

$$\dot{s}_2 = -C_1 n_e (B_y^2 - B_x^2) s_3 + C_3 n_e B_z s_1, \quad (41)$$

$$\dot{s}_3 = C_1 n_e (B_y^2 - B_x^2) s_2 - 2C_1 n_e B_x B_y s_1.$$

For the lateral chords, the z-axis is the direction of the laser beam propagation, and so the radial component B_r is parallel to the laser beam propagation direction, whereas the toroidal (B_t) and poloidal (B_v) components are orthogonal to the propagation direction. Equations (41) can be rewritten as

$$\dot{s}_1 = 2C_1 n_e B_v B_t s_3 - C_3 n_e B_r s_2,$$

$$\dot{s}_2 = -C_1 n_e (B_t^2 - B_v^2) \cdot s_3 + C_3 n_e B_r s_1, \quad (42)$$

$$\dot{s}_3 = C_1 n_e (B_t^2 - B_v^2) \cdot s_2 - 2 \cdot C_1 n_e B_v B_t s_1.$$

Starting from Eqs. (42) some considerations are necessary. Usually, in a tokamak, and thus also in JET, the toroidal magnetic field B_t is about two orders of magnitude higher than the other two components B_r and B_v. Therefore, neglecting the components of Eq. (42) that includes only B_z and B_r, the error in the evaluation of stokes components is less than 1%. With this approximation Eqs. (42) can be written as

$$\dot{s}_1 \cong 2C_1 n_e B_v B_t s_3,$$

$$\dot{s}_2 \cong -C_1 n_e (B_t^2 - B_v^2) s_3, \quad (43)$$

$$\dot{s}_3 = C_1 n_e (B_t^2 - B_v^2) s_2 - 2C_1 n_e B_v B_t s_1.$$

In this case the expressions (43), for the three components of Stokes vector, can be integrated numerically. The Stokes components resulting from propagation Eqs. (43) permit to evaluate the Faraday angle and the phase shift.[11]

In JET the laser beam of the lateral polarimeter chords is sent into the plasma with a linear polarization of 0° with respect to the toroidal magnetic field direction and therefore the initial Stokes vector is

$$s_0 = (1,0,0). \quad (44)$$

Taking into account the geometrical configuration of the magnetic field for the lateral chords, the Stokes vector can be written as

$$s(z) \approx (1, W_3, -W_2). \quad (45)$$

In the case that $|W_2|, |W_3| \ll 1$, the Eq. (45) represents a polarization rotated by an angle of $\delta\psi = W_3/2$ and whose ellipticity is given by $-W_2/2$.[11]

In this last form, it is possible to link the Faraday angle and the electronic density measurements. In the case of negligible variations in the radial component of the magnetic field along the torus radius, it is possible to write the Faraday angle and the phase shift as

$$\Psi = \tfrac{1}{2}\text{arctag}(W_3), \quad (46)$$

TABLE II. Statistical analysis, for all lateral chords, of the measurements of the electron density. Again the percentages of the estimates in acceptable agreement with the experimental measurements within one fringe are reported.

Statistical analysis on 200 shots–one fringe error (%)				
Chord	No. 5	No. 6	No. 7	No. 8
Far_th-interferom	56	64	61	44

$$\Phi = \text{arctag}(-W_2). \tag{47}$$

Since $W_3 = C_3 \int_{z_0}^{z} n(z) \cdot (B_r) dz$ the Faraday angle Ψ is proportional to the line integral of the electronic density and to the radial magnetic field B_r.

The numerical solutions of Eq. (42), or of the approximated form (43), for the lateral chords are in acceptable agreement with data of the Faraday angle and with the interferometer measurements. The summary of the statistical analysis on all lateral chords is given in Table II. In this case the shots available for the statistical analysis are smaller than the vertical ones due to hardware problems with the lateral views.

V. APPLICATION TO THE PLASMA MEASUREMENTS

Once obtained the calibration curves for the Faraday rotation and the phase shift, the experimental signals with plasma have been analyzed applying the new calibration code.

Starting from the raw data acquired, RMS, RMP, PSP, and PSD, one can obtain the components of Stokes vector,[8] which describes the polarization state of the beam passes through all the optical components and the plasma, using the following equations (see Sec. II):

$$RMS = \tfrac{1}{2} E_{H,0}^2, \tag{48}$$

$$RMP = \tfrac{1}{2} E_{H,0}'^2, \tag{49}$$

$$PSD = \tfrac{1}{2} E_{H,0}' \cdot E_{V,0} \cos\varphi, \tag{50}$$

$$PSP = \tfrac{1}{2} E_{H,0} \cdot E_{V,0} \cos\varphi, \tag{51}$$

where the $E_{H,0}$ and $E_{V,0}$ are the electric field components measured, respectively, with the H-detector and the V-detector (see Fig. 1) and φ is the phase shift between them.

Since the position of the output wire grid could be rotated with respect to the original reference axes, a rotation of its output components has to be performed to express them in the right coordinate system. To this purpose the electric field components after the wire grid analyzer have to be expressed by means of the following transformations:

$$E_x = \alpha \cdot E_{H,0} + \delta \cdot E_{V,0}, \tag{52}$$

$$E_y = -\delta \cdot E_{H,0} + \alpha \cdot E_{V,0}, \tag{53}$$

where α and δ are, respectively, the cosine and the sine of the wire grid angle in the torus coordinate system. Once derived the components of the electric field at the exit of the plasma, the final Stokes vector $(\vec{S}_1)$ can be calculated.[8]

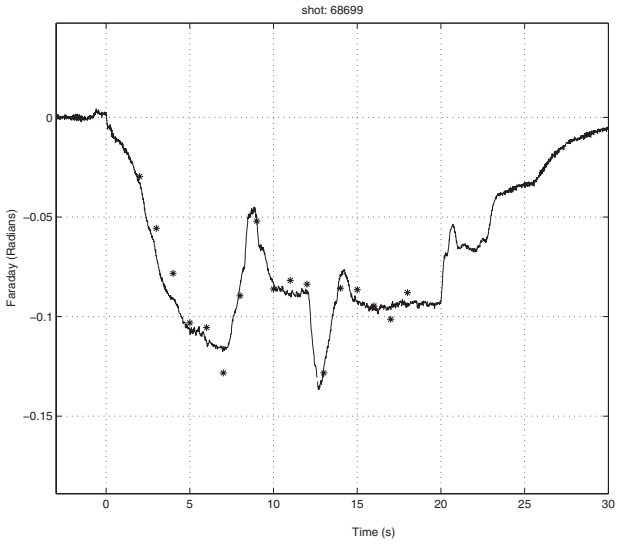

FIG. 9. Comparison Faraday angle: new calibration (continuous line) and numerical model (asterisks). Chord no. 2.

Hence, applying the calibration matrices to $\vec{S}_1$, it is possible to evaluate the plasma effects on the initial polarization state of laser beam, according to

$$\vec{S}_1 = M'_{\delta_2} \cdot M'_{\delta_1} \cdot M_\alpha \cdot M_{\text{plasma}} \cdot \vec{S}_0 \tag{54}$$

and thus

$$M_\alpha^{-1} \cdot M'^{-1}_{\delta_1} \cdot M'^{-1}_{\delta_2} \cdot \vec{S}_1 = M_{\text{plasma}} \cdot \vec{S}_0 \tag{55}$$

for the vertical chords. For the horizontal chords the relation is

$$M_\alpha^{-1} \cdot M_\varepsilon \cdot M'^{-1}_{\delta_1} \cdot M'^{-1}_{\delta_2} \cdot \vec{S}_1 = M_{\text{plasma}} \cdot \vec{S}_0. \tag{56}$$

After this procedure, the calibration parameter C, due to the signal processing electronics, is estimated. Since in absence of plasma the Faraday rotation must be equal to twice the half-wave angle, it is easy to find C comparing the experimental data (before 40 s) with this curve.

Figure 9 compares the Faraday rotation calculated with the new calibration code, with the results of a numerical model described in Sec. IV (asterisks). In Fig. 10 the same comparison for the phase shift is shown. The new calibration is in good agreement with the numerical solution. Figures 11–22 depict the results obtained for some shots acquired during the 2003–2007 experimental campaigns to show how the developed algorithm works satisfactorily for all chords.

Given the good results obtained for the earlier campaigns, the new calibration code has been applied to the shots performed during 2008–2009 and, also in this case, the comparison between the Stokes model outputs and the new calibration shows a good agreement.

On JET, for the vertical chords, it is easy to evaluate the density from the Cotton–Mouton measurements because the toroidal field (B_t) is largely constant along the line of sight, and thus Eq. (2) can be rewritten as

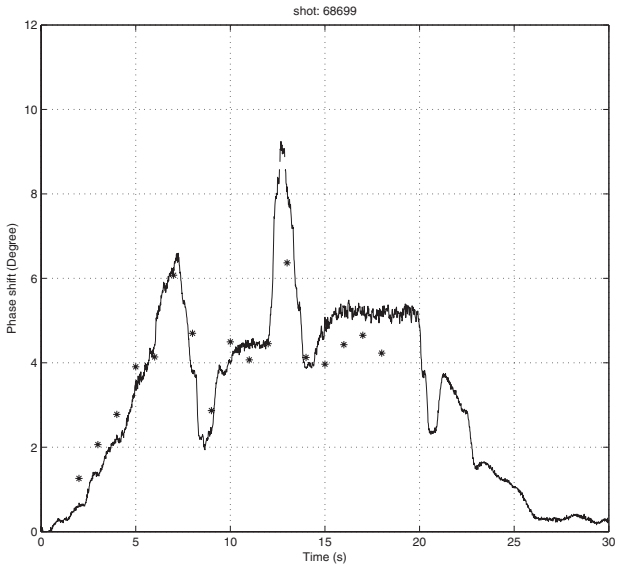

FIG. 10. Phase shift: comparison between the new calibration (continuous line) and numerical model (asterisks). Chord no. 2.

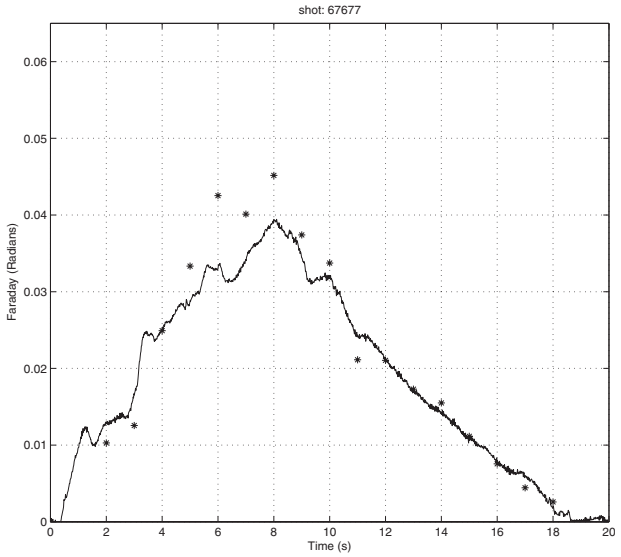

FIG. 11. Comparison Faraday angle: new calibration (continuous line) and numerical model (asterisks). Chord no. 3.

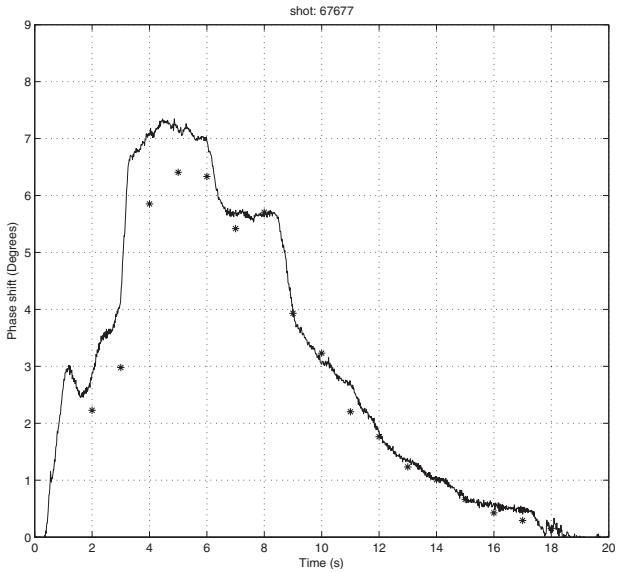

FIG. 12. Phase shift: comparison between the new calibration (continuous line) and numerical model (asterisks). Chord no. 3.

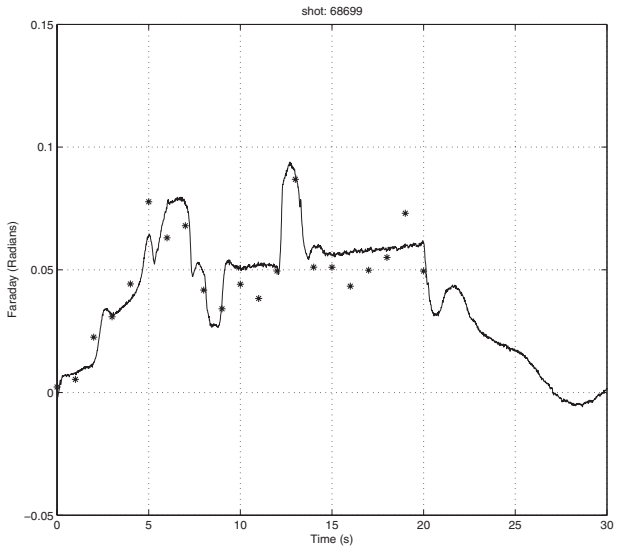

FIG. 13. Comparison Faraday angle: new calibration (continuous line) and numerical model (asterisks). Chord no. 4.

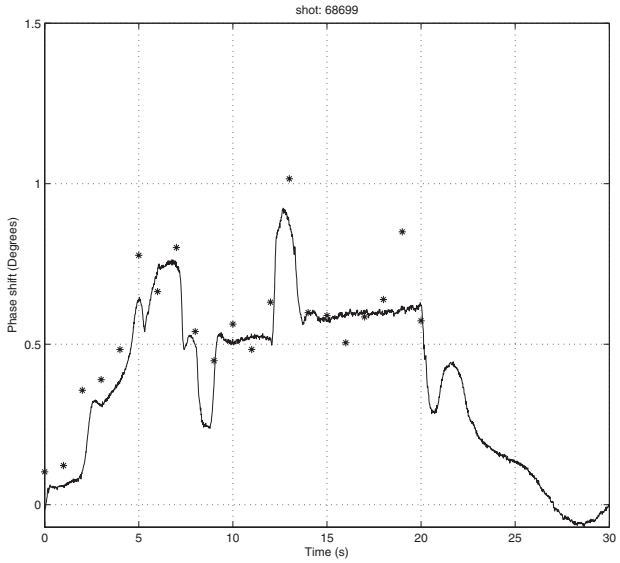

FIG. 14. Phase shift: comparison between the new calibration (continuous line) and numerical model (asterisks). Chord no. 4.

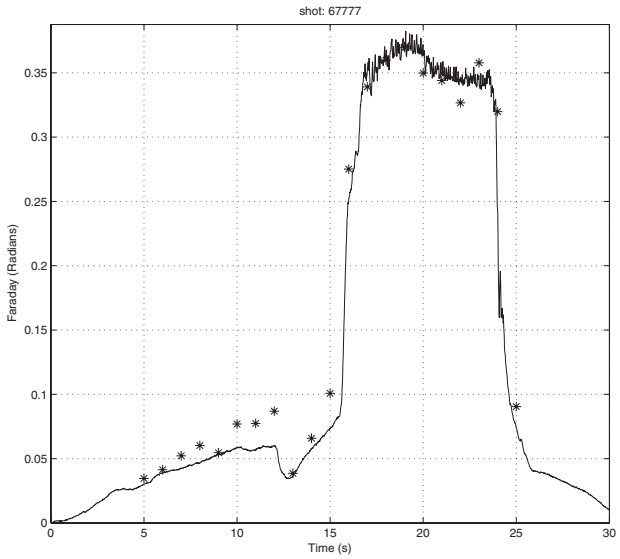

FIG. 15. Comparison Faraday angle: new calibration (continuous line) and numerical model (asterisks). Shot: 67777 chord no. 5.

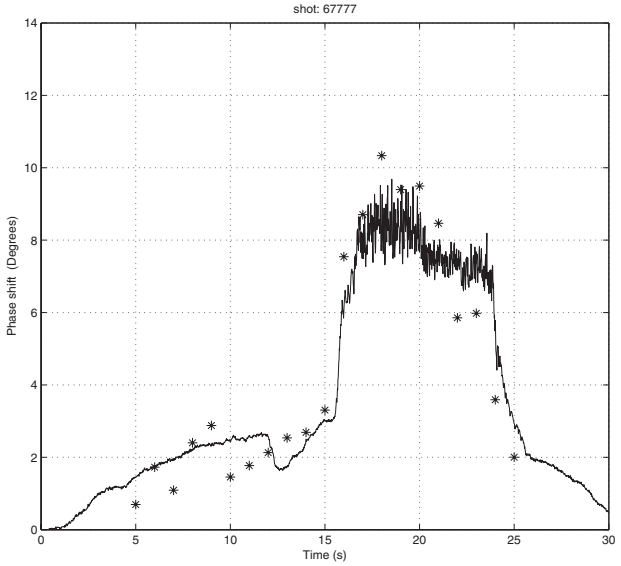

FIG. 16. Phase shift: comparison between the new calibration (continuous line) and numerical model (asterisks). Shot: 67777 chord no. 5.

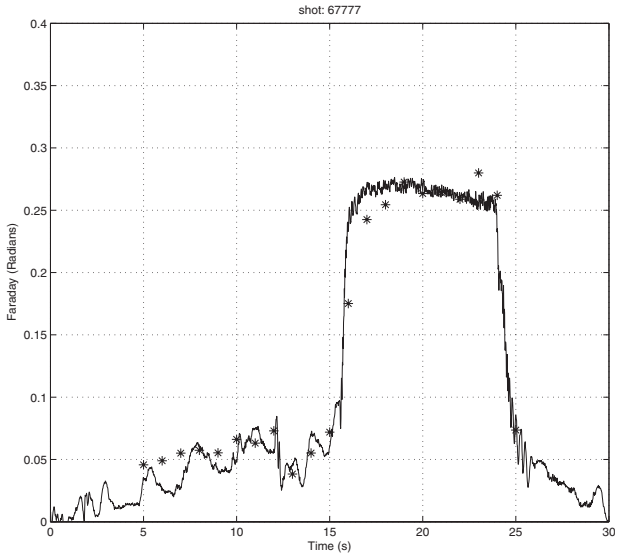

FIG. 17. Comparison Faraday angle: new calibration (continuous line) and numerical model (asterisks). Shot: 67777 chord no. 6.

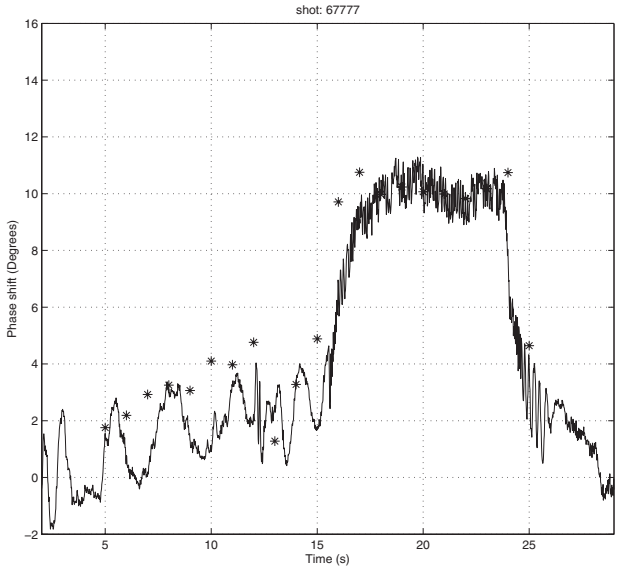

FIG. 18. Phase shift: comparison between the new calibration (continuous line) and numerical model (asterisks). Shot: 67777 chord no. 6.

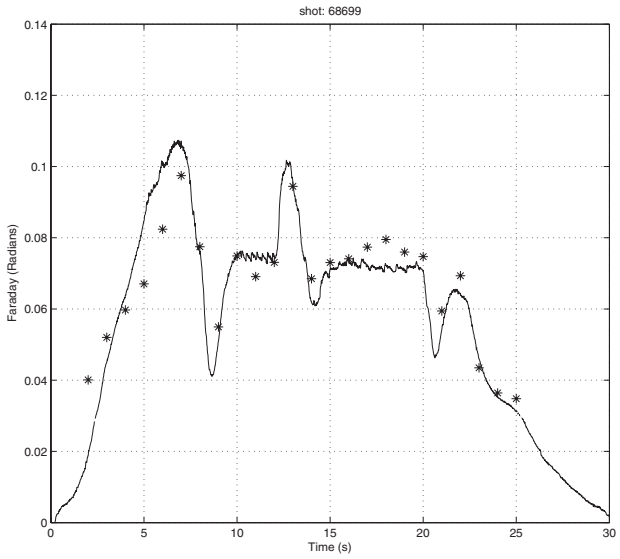

FIG. 19. Comparison Faraday angle: new calibration (continuous line) and numerical model (asterisks). Shot: 68699 chord no. 7.

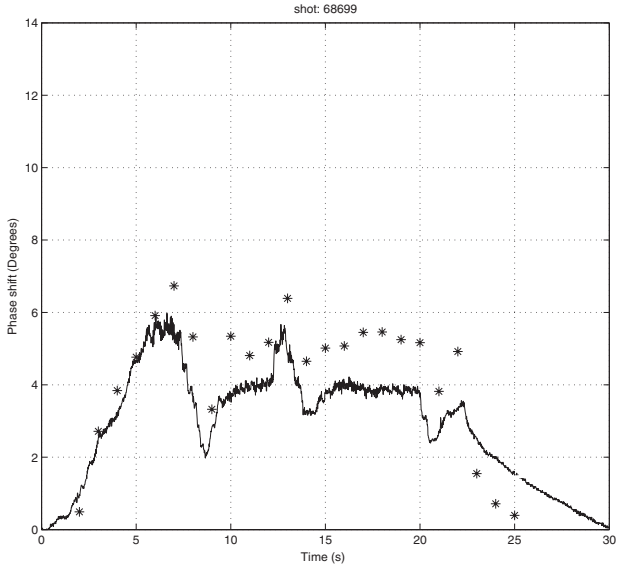

FIG. 20. Phase shift: comparison between the new calibration (continuous line) and numerical model (asterisks). Shot: 68699 chord no. 7.

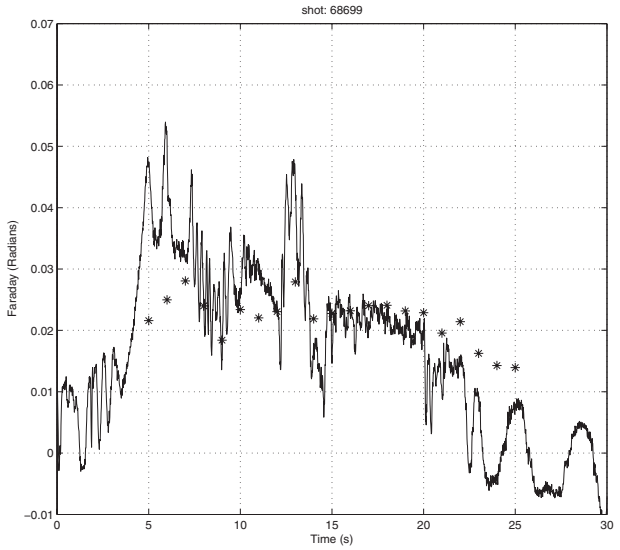

FIG. 21. Comparison Faraday angle: new calibration (continuous line) and numerical model (asterisks). Shot: 68699 chord no. 8.

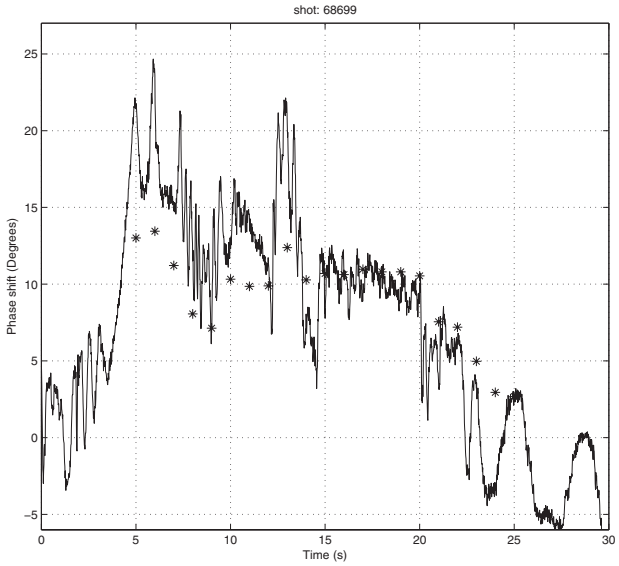

FIG. 22. Phase shift: comparison between the new calibration (continuous line) and numerical model (asterisks). Shot: 68699 chord no. 8.

$$\Phi = k \cdot \lambda^3 \cdot B_t^2 \cdot \int n_e \cdot dz \tag{57}$$

and therefore the line-integrated electron density (n_e) can be directly obtained

$$\int n_e \cdot dz = \frac{\Phi}{k \cdot \lambda^3 \cdot B_t^2}, \tag{58}$$

where k is a constant.

In the Figs. 23–25, the density calculated applying the new calibration code, for the vertical chords, is reported. The curve is compared with the computational model output and with the density measurement of the interferometer.

As it is clear, using the new calibration the density calculated with the polarimeter and with the interferometer are in good agreement.

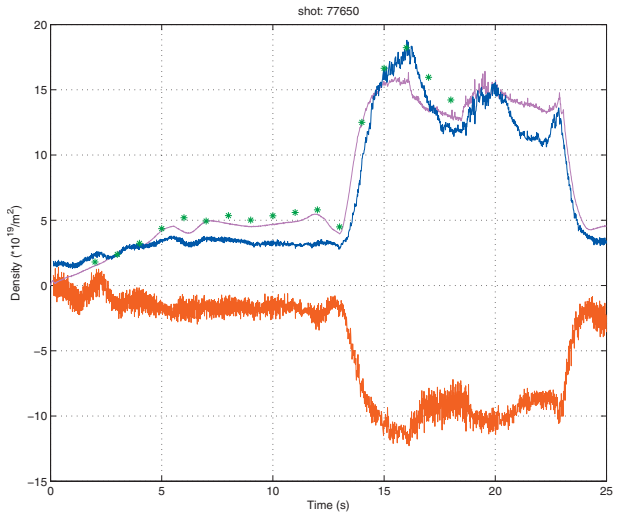

FIG. 23. (Color) Comparison between the density with the new calibration (blue line), the interferometer density (magenta line), the numerical model (asterisk), and the old calibration (red line). Shot: 77650 chord no. 2.

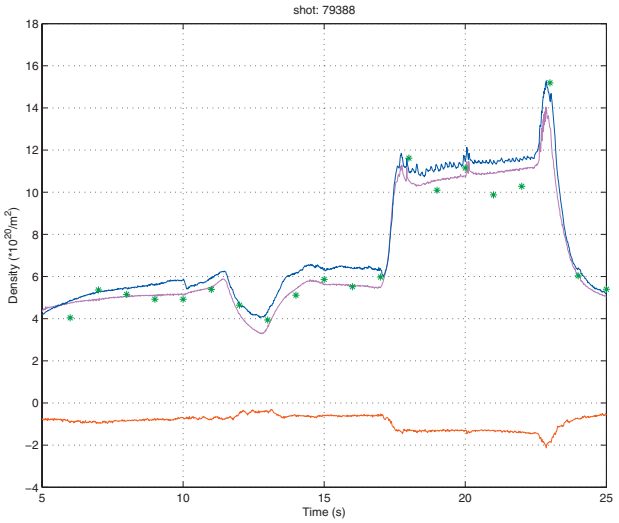

FIG. 24. (Color) Comparison between the density with the new calibration (blue line), the interferometer density (magenta line), the numerical model (asterisks), and the old calibration (red line). Shot: 79388 chord no. 3.

VI. CONCLUSIONS

JET polarimeter has been analyzed to understand and to solve the problems posed by the spurious ellipticity induced by the instrument optical components. Two analyses have been performed:

(1) check of the signal processing electronics to exclude additional anomalous behaviors;
(2) development of a new calibration code.

A simulator has been developed to verify the proper operation of the electronics. The analysis shows a very good agreement between the simulation outputs and the experimental data. Therefore, we can conclude that the signal processing electronics is still working within its design parameters.

After this analysis, a new calibration code has been written and tested for many shots acquired in different cam-

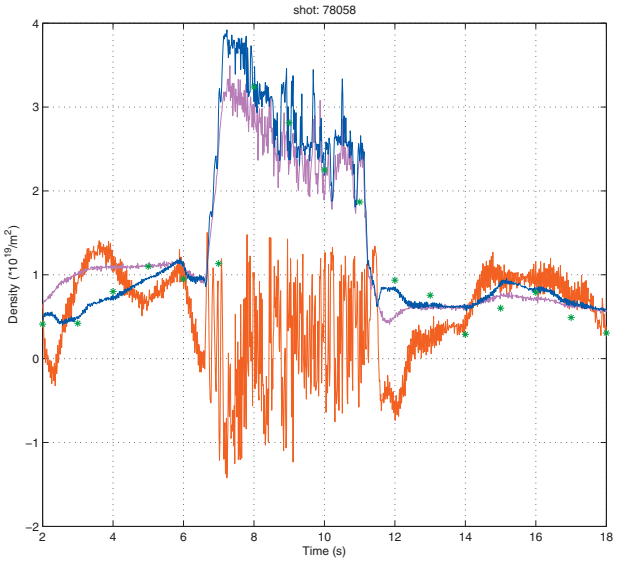

FIG. 25. (Color) Comparison between the density with the new calibration (blue line), the interferometer density (magenta line), the numerical model (asterisks), and the old calibration (red line). Shot: 78058 chord no. 4.

paigns. The experimental data, calibrated with this code, have been compared with the rigorous numerical solution of the Stokes equations. The obtained results show that the two estimates are in good agreement for both the Faraday rotation and the Cotton–Mouton effect. Moreover, starting from the phase shift obtained with this new code, the electron density has been evaluated for the vertical channels and compared with the density measured by the interferometer. The comparison with the experimental measurements confirms the quality of the developed calibration procedure.

ACKNOWLEDGMENTS

This work, supported by the European Communities under the contract of Association between EURATOM and ENEA, was carried out under the framework of the European Fusion Development Agreement. The views and opinions expressed herein do not necessarily reflect those of the European Commission.

[1] D. Goldstein, *Polarized Light* (CRC, Boca Raton, 2003).
[2] F. De Marco and S. Segre, Plasma Phys. **14**, 245 (1972).
[3] K. Guenther, Proceedings of the 31st EPS, 2004, P5–172.
[4] K. Guenther, Plasma Phys. Controlled Fusion **46**, 1423 (2004).
[5] C. Brault, CEA Cadarache, Internal Mission report, March 2009.
[6] M. Gelfusa, M. Brombin, P. Gaudio, A. Boboc, A. Murari, and F. P. Orsitto, "Modelling of the signal processing electronics of JET interferometer-polarimeter," Nucl. Instrum. Methods Phys. Res. (in press).
[7] See http://www.tina.com/English/tina for the detailed description of the software package designed to simulate electronic circuits.
[8] M. Born and E. Wolf, *Principles of Optics* (Pergamon, Oxford, 1980).
[9] D. S. Kliger, J. W. Lewis, and C. E. Randall, *Polarized Light in Optics and Spectroscopy* (Academic, San Diego, 1990).
[10] S. E. Segre, Plasma Phys. Controlled Fusion **35**, 1261 (1993).
[11] S. E. Segre, Plasma Phys. Controlled Fusion **41**, R57 (1999).
[12] F. De Marco and S. E. Segre, Opt. Commun. **23**, 125 (1977).
[13] F. P. Orsitto, A. Boboc, C. Mazzotta, E. Giovannozzi, and L. Zabeo, Plasma Phys. Controlled Fusion **50**, 115009 (2008).